First-principles study of defect equilibria in lithium zinc nitride

2007 J. Phys.: Condens. Matter 19 046201

(http://iopscience.iop.org/0953-8984/19/4/046201)

INSTITUTE OF PHYSICS PUBLISHING JOURNAL OF PHYSICS: CONDENSED MATTER

J. Phys.: Condens. Matter **19** (2007) 046201 (11pp) doi:10.1088/0953-8984/19/4/046201

First-principles study of defect equilibria in lithium zinc nitride

K Toyoura, F Oba, T Ninomiya, A Kuwabara and I Tanaka

Department of Materials Science and Engineering, Kyoto University, Kyoto 606-8501, Japan

E-mail: k.toyoura@t01a0005531.mbox.media.kyoto-u.ac.jp

Received 18 September 2006, in final form 4 December 2006
Published 12 January 2007
Online at stacks.iop.org/JPhysCM/19/046201

Abstract

First-principles calculations are performed in order to investigate defect equilibria in lithium zinc nitride (LiZnN). The formation energies of native defects and their thermal equilibrium concentrations are evaluated, considering vacancies, interstitials, and cation anti-site defects under relevant conditions of chemical potentials. It is clarified that acceptor-like Li anti-sites are dominant under ordinary p_{N_2}–T conditions. The concentrations of donor-like defects, which can compensate the negative charge of ionized Li anti-sites, are much lower. This results in the formation of holes with a high concentration even in undoped LiZnN.

1. Introduction

$A^+B^{2+}X^{3-}$-type compounds, which are sometimes referred to as Nowotny–Juza (NJ) compounds, have been systematically synthesized since the middle of the 20th century [1–6]. In the NJ compounds, B^{2+} and X^{3-} form a framework of the zinc blende structure. As shown in figure 1(a), the B^{2+} and X^{3-} are located at (0, 0, 0; 0, 1/2, 1/2; 1/2, 0, 1/2; 1/2, 1/2, 0) and (1/4, 1/4, 1/4; 1/4, 3/4, 3/4; 3/4, 1/4, 3/4; 3/4, 3/4, 1/4), respectively. A^+ occupies a tetrahedral interstitial site, either Int_1 at (1/2, 1/2, 1/2; 1/2, 0, 0; 0, 1/2, 0; 0, 0, 1/2) or Int_2 at (3/4, 3/4, 3/4; 3/4, 1/4, 1/4; 1/4, 3/4, 1/4; 1/4, 1/4, 3/4), coordinated by four X^{3-} anions or B^{2+} cations. The resultant structure has a cubic lattice with a space group of $F\bar{4}3m$. The optical and electrical properties of various NJ compounds (LiZnN, LiZnP, LiZnAs, LiMgN, etc) have been experimentally investigated by Kuriyama *et al* and Bacewicz *et al* successively since 1987 [7–14]. They reported that most of the NJ compounds show p-type conductivity.

Lithium zinc nitride (LiZnN) is one of the NJ compounds; it has been synthesized by heating a mixture of lithium nitride (Li_3N) and zinc nitride (Zn_3N_2) in a flow of NH_3 [3], or by a direct reaction between NH_3 and LiZn [7, 8]. The crystal structure is shown in figure 1(b). Li^+ occupies the Int_1 site surrounded by four N^{3-} anions. Kuriyama *et al* evaluated the optical properties by photo-transmittance measurements and photo-acoustic spectroscopy [7, 8], revealing that LiZnN has a direct bandgap of about 1.9 eV. Although the

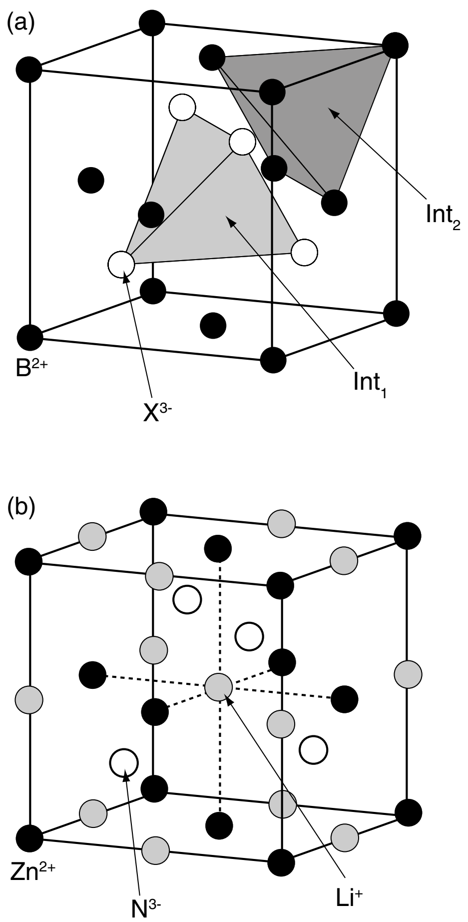

Figure 1. Crystal structures of (a) Nowotny–Juza compounds and (b) LiZnN.

electrical properties of LiZnN have not been well understood, the direct bandgap is of interest in view of applications in optoelectronics.

In this work, we investigate native defect equilibria in LiZnN using first-principles calculations. Although the electronic structure of the perfect LiZnN crystal has been theoretically elucidated [15, 16], calculations on the native defects have not been reported. The formation energies and thermal equilibrium concentrations of native defects are calculated under relevant conditions of chemical potentials. Based on the results, defect species that can be closely related to the electrical properties are discussed.

2. Calculation methods

2.1. Electronic structure and total energy

The calculations were performed using a first-principles projector augmented wave (PAW) method [17] as implemented in VASP code [18–22]. For the exchange correlation, we employed the generalized-gradient approximation parameterized by Perdew, Burke and Ernzerhof (GGA-PBE) [23]. The plane wave cut-off energy was set to be 500 eV. 2s 2p for Li, 3d 4s for Zn and 2s 2p for N were treated as valence.

Prior to defect calculations, the electronic structure of the perfect LiZnN crystal was investigated. We used the primitive cell (three atoms) and Brillouin zone integration was made using a $6 \times 6 \times 6$ k-point mesh (28 irreducible k-points) according to the Monkhorst–Pack scheme [24]. The calculated lattice constant, 4.93 Å, is within typical GGA errors from experimental values, 4.88 Å [3], 4.91 Å [7], and 4.90 Å [8]. Calculating the total energy of a defective cell, we used a 324-atom supercell, constructed by $3 \times 3 \times 3$ expansion of the unit cell, and a single k-point sampling at the Γ point. The atomic positions were fully relaxed according to the Hellmann–Feynman forces [25] until the residual forces converged to be less than 0.05 eV Å^{-1}.

2.2. Formation energy and concentration of native defects

The formation energy of a defect in a charge state q is defined as [26]

$$E^{\text{defect}}_{\text{form}}(q) = E^{\text{defect}}_{\text{total}}(q) - \sum_l n_l \mu_l + q[\varepsilon_{\text{F}} + E_{\text{VBM}}], \tag{1}$$

where $E^{\text{defect}}_{\text{total}}(q)$ is the total energy of a defective cell, n_l is the number of l atoms in the defective cell, μ_l is the chemical potential of atom l in LiZnN, and ε_{F} is the Fermi level measured from the valence band maximum (E_{VBM}). The difference between E_{VBM} of the charged defective cell and that of the perfect cell was corrected using average electrostatic potentials for atoms in accordance with [27].

The calculated defect formation energy may include some errors because GGA (and LDA) generally tends to underestimate the bandgap energy. Actually, our result for the perfect LiZnN cell, which will be detailed in section 3.1, shows that the bandgap is underestimated by 1.4 eV. If a defect level has an orbital character similar to the conduction band, it should be also underestimated. In such cases, as is often the case with donor-like defects, the formation energy can be corrected as follows:

$$E_{\text{form}}(q;\,\text{corrected}) = E_{\text{form}}(q;\,\text{calculated}) + m\Delta E_{\text{g}}, \tag{2}$$

where m is the number of electrons occupied at the defect level, and ΔE_{g} is the difference between the experimental and calculated bandgaps (1.4 eV).

The thermal equilibrium defect concentration can be given by

$$C^{\text{defect}} = N_{\text{site}} N_{\text{config}} \exp\left(-\frac{E^{\text{defect}}_{\text{form}}(q)}{k_{\text{B}}T}\right). \tag{3}$$

N_{site} and N_{config} are the numbers of sites per unit volume and of equivalent configurations for the defect, k_{B} is the Boltzmann constant, and T is the temperature. Electron and hole concentrations (n and h) can be evaluated by following equations:

$$n = 2\left(\frac{m_{\text{e}}kT}{2\pi\hbar^2}\right)^{3/2} \exp[(\varepsilon_{\text{F}} - E_{\text{g}})/kT], \tag{4}$$

$$h = 2\left(\frac{m_{\text{h}}kT}{2\pi\hbar^2}\right)^{3/2} \exp[-\varepsilon_{\text{F}}/kT], \tag{5}$$

where E_{g} is the bandgap, and m_{e} and m_{h} are the effective masses of the electron and hole, respectively. For E_{g}, the experimental value of 1.9 eV [7, 8] was used. m_{e} and m_{h} were obtained from the curvatures of bands near the valence band maximum (VBM) and the conduction band maximum (CBM), by the following equation:

$$\frac{1}{m^*} = \frac{1}{\hbar}\frac{\mathrm{d}^2\varepsilon}{\mathrm{d}k^2}. \tag{6}$$

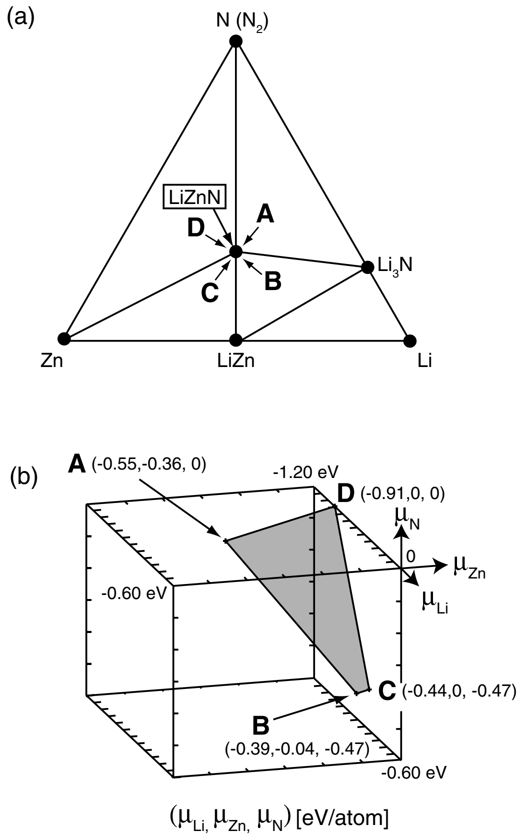

Figure 2. (a) Schematic phase diagram for the Li–Zn–N system. A–D correspond to the equilibrium conditions of LiZnN–N_2–Li_3N, LiZnN–Li_3N–LiZn, LiZnN–LiZn–Zn, and LiZnN–Zn–N_2, respectively. (b) The range of chemical potentials where LiZnN is stable. A–D mean the same equilibrium conditions as in figure 2(a).

Defect concentrations under respective conditions of chemical potentials (μ_{Li}, μ_{Zn}, μ_{N}) can be obtained using the charge neutrality condition, which is given by

$$h - n + \sum_{\text{defect}} qC^{\text{defect}}(q) = 0. \tag{7}$$

2.3. Atomic chemical potentials

The chemical potential of each element must be specified in calculating the defect formation energies. First of all, μ_{Li}, μ_{Zn}, and μ_{N} in LiZnN are constrained by the following condition:

$$\mu_{\mathrm{Li}} + \mu_{\mathrm{Zn}} + \mu_{\mathrm{N}} = \mu_{\mathrm{LiZnN}}, \tag{8}$$

where μ_{LiZnN} is the chemical potential of LiZnN. μ_{LiZnN} was replaced by the calculated total energy of the perfect LiZnN crystal. Assuming equilibrium states among three phases, μ_{Li}, μ_{Zn} and μ_{N} can be uniquely determined. Since experimental phase diagrams are not available for the Li–Zn–N system, we determined the phase equilibria using calculated total energies of metallic Li and Zn, N_2 gas, LiZn, Li_3N and Zn_3N_2. The result is shown in figure 2(a). Zn_3N_2 was calculated to be unstable at the ground state and therefore does not appear in the figure. Four equilibrium conditions are found, which are (A) LiZnN–N_2–Li_3N, (B) LiZnN–Li_3N–LiZn, (C) LiZnN–LiZn–Zn, and (D) LiZnN–Zn–N_2. These conditions correspond to the limits of the chemical potentials. When the references for the chemical potentials are defined as

$$\mu_{\mathrm{Li}}(\text{in Li}) = 0, \qquad \mu_{\mathrm{Zn}}(\text{in Zn}) = 0, \qquad \mu_{\mathrm{N}}(\text{in } \mathrm{N}_2) = 0, \tag{9}$$

μ_{Li}, μ_{Zn} and μ_{N} at 0 K vary within the shaded area as indicated in figure 2(b). If other equilibrium phases were considered, the stable region of LiZnN would become smaller.

In the present study, we take into account the temperature dependence of the chemical potentials of the nitrogen gas phase (N_2(g)), which is expected to have much greater temperature dependence than those of solid phases. Using the ideal gas approximation, the temperature dependence of the nitrogen chemical potential is given by

$$\mu_{\mathrm{N}} = \tfrac{1}{2}[E_{\mathrm{N}_2} + \tfrac{1}{2}h\nu + kT\ln(pV_Q/kT) - kT\ln Z_{\mathrm{rot}} - kT\ln Z_{\mathrm{vib}}], \tag{10}$$

where E_{N_2} is the electronic energy of a nitrogen molecule, $1/2h\nu$ is the zero-point vibrational energy, and p is the pressure. V_Q is the quantum volume defined as $(h^2/2\pi mkT)^{3/2}$. Z_{rot} and Z_{vib} are the rotational and vibrational partition functions. E_{N_2} was replaced by the calculated total energy. Z_{rot} was obtained using the model of a rigid rotor, and the eigenfrequency ν and Z_{vib} were evaluated by means of the frozen phonon method combined with first-principles calculations [28]. The temperature dependence of the nitrogen chemical potentials obtained by equation (10) agrees with the experimental values within an error of 0.1% up to 3000 K under atmospheric pressure (10^5 Pa) [29].

3. Results and discussion

3.1. Electronic structure of perfect LiZnN

Figure 3 shows the calculated electronic band structure and density of states (DOS) of the perfect LiZnN crystal. Calculations of projected DOS indicate that the lowest band located at −14.5 to −13.0 eV corresponds to N 2s states. Zn 3d and N 2p states lie at −7.0 to −5.5 eV and −5.5 to 0.0 eV, respectively. The conduction band is mainly composed of Li 2sp and Zn 4sp. Both the VBM and CBM are located at Γ point, giving a direct gap in consistency with previous experimental [7] and theoretical [15, 16] reports. The calculated bandgap energy is 0.53 eV, which is underestimated by about 1.4 eV as compared with experimental values of about 1.9 eV [7, 8].

The carrier effective masses in LiZnN were estimated from the curvatures of bands near the VBM and CBM. The electron and light hole effective masses were found to be nearly isotropic, both about $0.2m_0$, where m_0 is the mass of a free electron. On the other hand, the heavy hole showed a strong anisotropy, $0.9m_0$ and $1.9m_0$ in the L-direction and in X-direction, respectively.

3.2. Formation energy of native defects

We computed the formation energies at 0 K of the vacancies (V_{Li}, V_{Zn}, and V_{N}), the tetrahedral interstitials (Int_2) (Li_i, Zn_i, and N_i), and the cation anti-site defects ($\mathrm{Zn}_{\mathrm{Li}}$ and $\mathrm{Li}_{\mathrm{Zn}}$), including corrections as given in equation (2). Figures 4 show the resultant formation energies as a function of the Fermi level ε_{F} under the equilibrium conditions of (a) LiZnN–N_2–Li_3N, (b) LiZnN–Li_3N–LiZn, (c) LiZnN–LiZn–Zn, and (d) LiZnN–Zn–N_2, respectively. In these figures, the zinc and nitrogen interstitials are not shown because of their extremely high formation energies, which are more than 5.5 eV with neutral charge states under all equilibrium

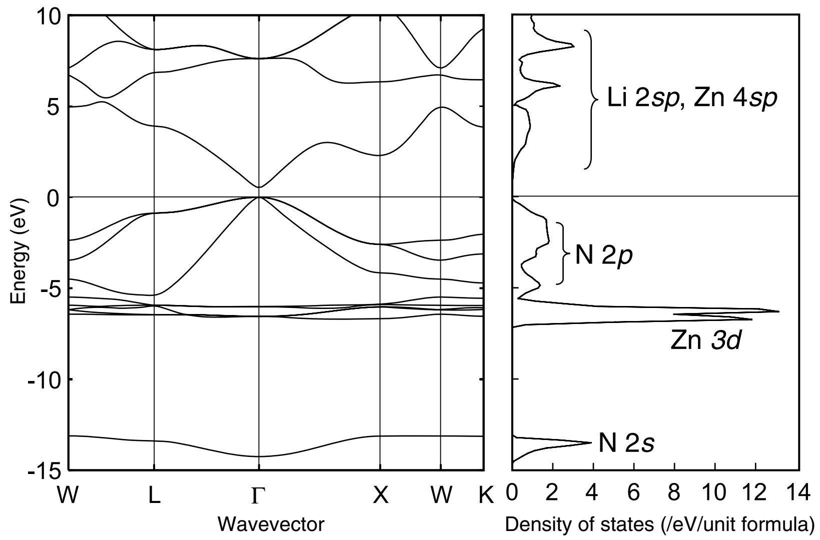

Figure 3. Electronic band structure and density of states (DOS) of perfect LiZnN. The valence band maximum is set to be zero.

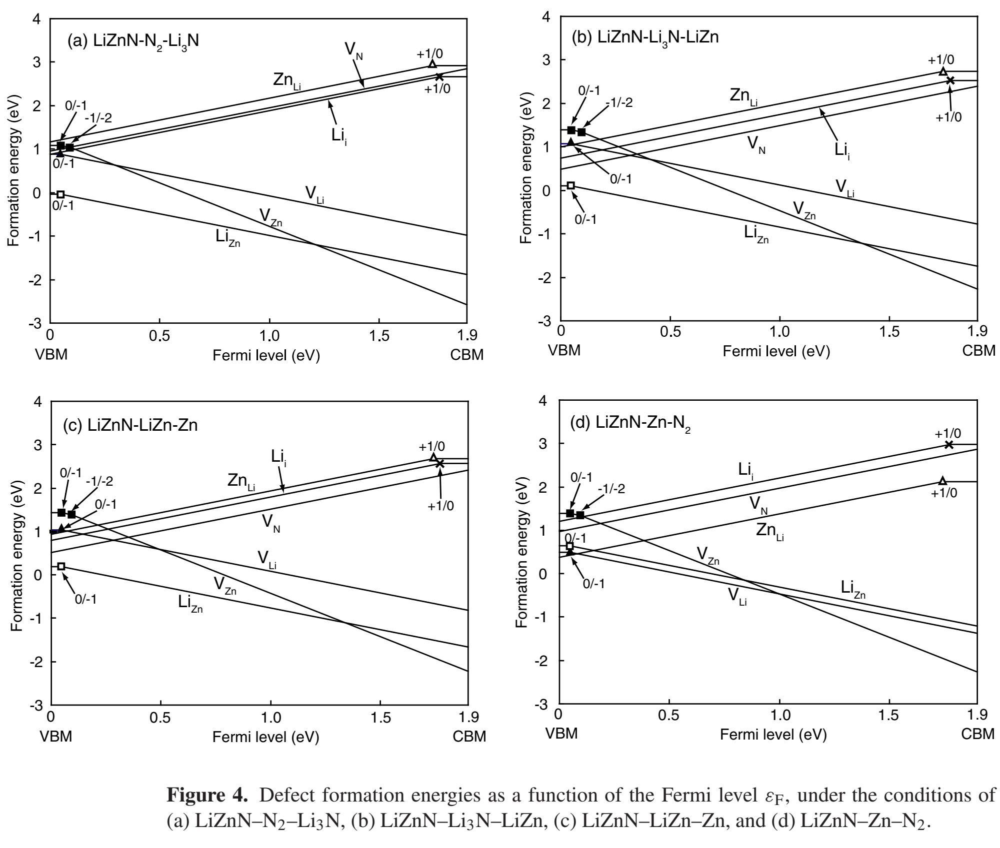

Figure 4. Defect formation energies as a function of the Fermi level ε_F, under the conditions of (a) LiZnN–N_2–Li_3N, (b) LiZnN–Li_3N–LiZn, (c) LiZnN–LiZn–Zn, and (d) LiZnN–Zn–N_2.

conditions. Only the most stable charge state of each defect species is plotted against ε_F. According to the definition of formation energy in equation (1), the gradient of formation

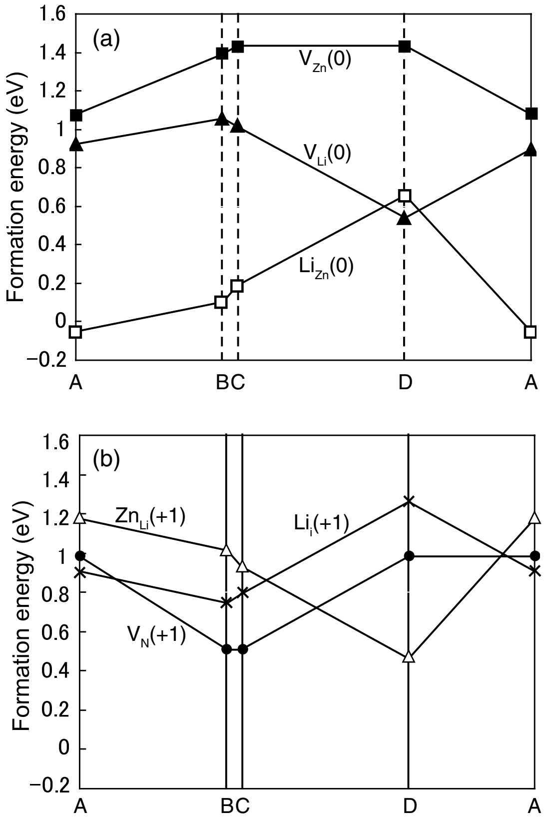

Figure 5. The formation energies of (a) acceptor- and (b) donor-like defects with the Fermi level located at the valence band maximum. The horizontal axis corresponds to equilibrium states along the lines around the shaded area in figure 2(b).

energy corresponds to the charge state, q. The defect transition level can be described as the point of change in slope, where two charge states show the same formation energies. Positive gradient means that the defect is a donor type, whereas negative shows an acceptor type.

Figure 4(a) indicates that under the Li- and N-rich condition, the most dominant defect is a substituted Li for Zn (Li_{Zn}), i.e., the Li anti-site, when ε_F is close to the VBM. The formation energy of $V_{Zn}(-2)$ is equal to that of $Li_{Zn}(-1)$ at $\varepsilon_F \approx 1.2$ eV, and V_{Zn} shows the lowest formation energy with ε_F near the CBM. Among the donor-like defects, the lithium interstitial Li_i is the most stable one in the whole range of ε_F; however, it is energetically less favourable than the acceptor-like defects. Under the N-poor conditions shown in figure 4(b) or (c), the formation energies of the donor-like defects become relatively low compared with the N- and Li-rich condition A. Still, they remain higher in energy than the acceptor-like Li_{Zn}.

In the phase equilibrium condition of LiZnN–Zn–N_2 shown in figure 4(d), it should be noted that the formation energy of V_{Li} is lower than that of Li_{Zn} over the whole range of ε_F, and that the donor-like Zn_{Li} is the most dominant defect near the VBM. Figures 5(a) and (b) show the formation energies of acceptor- and donor-like defects when ε_F is located at the VBM. The horizontal axis corresponds to equilibrium states along the lines surrounding the shaded area in figure 2(b). Acceptor-like Li_{Zn} has the lowest formation energy in almost the whole range of chemical potentials. Zn_{Li} and V_{Li} are energetically more favourable only near the condition D.

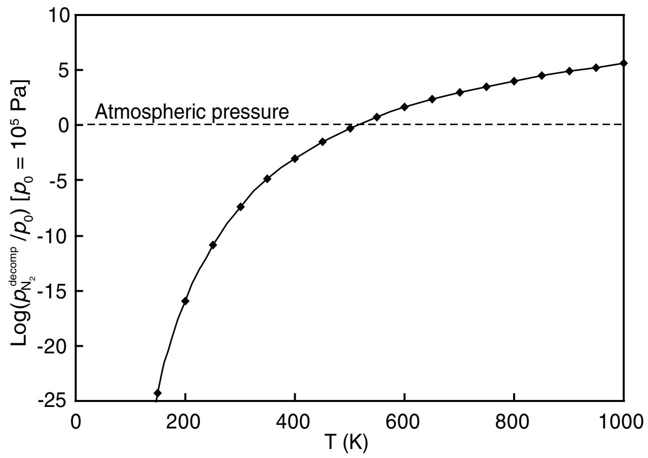

Figure 6. Calculated decomposition nitrogen partial pressure as a function of the temperature.

3.3. Thermal equilibrium concentrations of native defects

In this section, we discuss the dependences of the thermal equilibrium concentrations of native defects on the temperature T and nitrogen partial pressure p_{N_2}. We focus on the equilibrium condition D, because equation (3) should not be applied for the other conditions, where the cation ratio (Li/Zn) of LiZnN is expected to deviate far from the stoichiometric composition due to the low or negative formation energy of $\mathrm{Li_{Zn}}$.

Before investigating the T and p_{N_2} dependences of the defect formation, we confirmed the thermal stability of LiZnN with respect to the reference phases such as Zn and LiZn. At elevated temperatures or low p_{N_2}, μ_N of nitrogen gas decreases according to equation (10), and then the value of μ_N under the condition D gradually comes close to that of C at 0 K, -0.47 eV in figure 2(b). Finally, the stable region of LiZnN vanishes when μ_N of nitrogen gas becomes lower than -0.47 eV. This situation can be expressed by the following relation:

$$\mu_{\mathrm{LiZnN}} > \mu_{\mathrm{LiZn}} + \tfrac{1}{2}\mu_{N_2}, \tag{11}$$

which means the decomposition of LiZnN into LiZn and N_2 gas. Figure 6 shows the calculated decomposition nitrogen partial pressure $p_{N_2}^{\mathrm{decomp}}$ as a function of the temperature. This pressure corresponds to the lower limit of stable conditions for LiZnN. LiZnN decomposes at temperatures higher than ~500 K under atmospheric partial nitrogen pressure, which is comparable with the report that LiZnN decomposes at 773 K in a stream of nitrogen and hydrogen mixed gas (without description of the N_2/H_2 ratio) [3].

Figure 7 is a plot of the defect and carrier concentrations against the Fermi level ε_F under the standard condition of $p_{N_2} = 10^5$ Pa and $T = 298$ K. As a result of charge neutralization, the cross point of the $\mathrm{Li_{Zn}}(-1)$ and hole lines approximately gives the Fermi level ($\varepsilon_F = 0.15$ eV) and their concentrations (3×10^{17} cm^{-3}) under the thermal equilibrium state. The most dominant defect, acceptor-like $\mathrm{Li_{Zn}}(-1)$, and holes predominantly compensate their charges with each other, because the other defects are not formed in substantial concentrations due to their high formation energies. The p_{N_2} dependence of the concentrations of defects and carriers at room temperature (298 K) is shown in figure 8. In the whole range of p_{N_2} from 10^{-2} to 10^8 Pa, $\mathrm{Li_{Zn}}$ is the major defect, and the Fermi level is located near the VBM. At higher p_{N_2}, under which μ_{Li} decreases and μ_N increases, the formation energy of $\mathrm{Li_{Zn}}$ becomes higher and the Fermi level shifts to higher energy. This is why the concentration

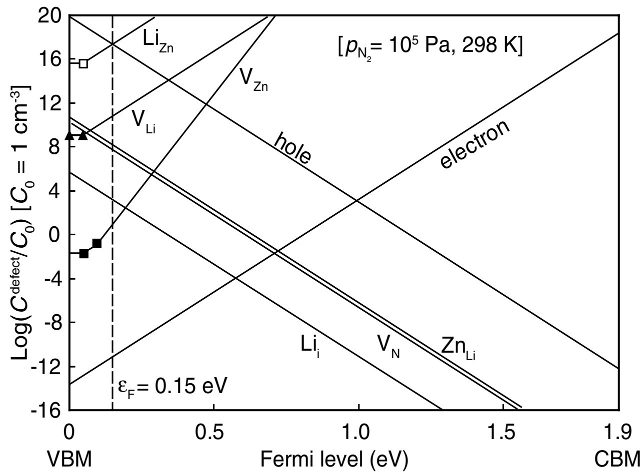

Figure 7. Defect and carrier concentrations as a function of the Fermi level under the standard condition of $p_{N_2} = 10^5$ Pa and $T = 298$ K.

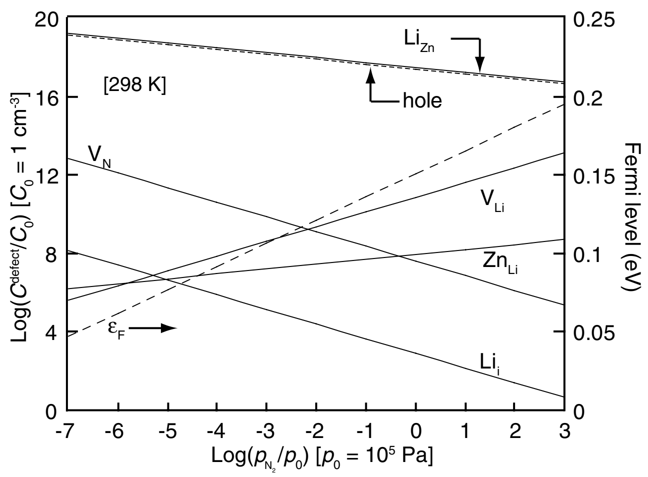

Figure 8. p_{N_2} dependences of the thermal equilibrium concentrations of defects and holes, and Fermi level at room temperature (298 K).

of the dominant acceptor-type defect $Li_{Zn}(-1)$ decreases as p_{N_2} becomes higher. Figure 9 shows the temperature dependence of defects and carrier concentrations under atmospheric p_{N_2} of 10^5 Pa. The concentrations of all defects increase with elevating temperature, and that of the dominant defect Li_{Zn} reaches 5×10^{20} cm^{-3} at 500 K. At temperatures higher than 500 K, LiZnN decomposes into LiZn and N_2 gas within the present calculations, as described in figure 6.

These results revealed that acceptor-like Li_{Zn} is the major defect under the ordinary p_{N_2}–T range in the equilibrium condition D, i.e., LiZnN–Zn–N_2, although the formation energy of the lithium vacancy V_{Li} is the lowest at 0 K. Under the other conditions, Li_{Zn} has lower formation energy than that under the condition D, and is evidently dominant, as recognized in figures 4 and 5. Therefore, Li_{Zn} is considered to be the major defect in most of thermal

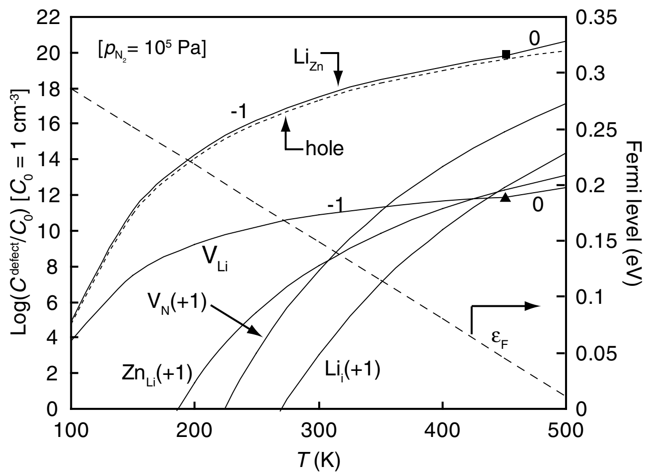

Figure 9. Temperature dependences of defects and hole concentrations, and Fermi level under atmospheric nitrogen partial pressure ($p_{N_2} = 10^5$ Pa).

equilibrium conditions. This suggests that LiZnN grown under ordinary conditions shows p-type conductivity. Although no experimental reports on electric conductivity can be found for LiZnN, other NJ compounds, such as LiZnP or LiZnAs, have been experimentally reported to show p-type conductivity [9, 11].

4. Conclusions

We have investigated defect equilibria in LiZnN using a first-principles PAW method. The substituted lithium for zinc, Li_{Zn}, is found to be the most dominant defect in most thermal equilibrium conditions. The concentration of Li_{Zn} increases as the nitrogen partial pressure becomes lower and the temperature becomes higher, to reach 5×10^{20} cm^{-3} at 500 K under the equilibrium condition of LiZnN–Zn–N_2 ($p_{N_2} = 10^5$ Pa). As Li_{Zn} is an acceptor-like defect, LiZnN prepared in thermal equilibrium conditions is likely to show p-type conductivity.

Acknowledgments

The authors would like to thank Togo A for helpful discussions. This work was supported by the 21st century COE program and a Grant-in-Aid for Young Scientists (B) from the Ministry of Education, Culture, Sports, Science and Technology of Japan.

References

[1] Nowotny H and Sibert W 1941 *Z. Metall.* **33** 391
[2] Juza R and Hund F 1946 *Naturwissenschaften* **33** 121
[3] Juza R and Hund F 1948 *Z. Anorg. Alleg. Chem.* **257** 1
[4] Nowotny H and Bachmayer K 1949 *Monatsh. Chem.* **80** 734
[5] Nowotny H and Bachmayer K 1950 *Monatsh. Chem.* **81** 488
[6] Nowotny H and Bachmayer K 1950 *Monatsh. Chem.* **81** 669
[7] Kuriyama K, Kato T and Tanaka T 1994 *Phys. Rev.* B **49** 4511
[8] Kuriyama K, Taguchi R, Kushida K and Ushiyama K 1999 *J. Cryst. Growth* **198/199** 802
[9] Kuriyama K and Nakamura F 1987 *Phys. Rev.* B **36** 4439

[10] Bacewicz R and Ciszek F T 1988 *Appl. Phys. Lett.* **52** 1150
[11] Kuriyama K, Katoh T and Mineo N 1991 *J. Cryst. Growth* **108** 37
[12] Kuriyama K, Kushida K and Taguchi R 1998 *Solid State Commun.* **108** 429
[13] Kuriyama K and Kushida K 2000 *J. Appl. Phys.* **87** 3168
[14] Kuriyama K, Nagasawa K and Kushida K 2002 *J. Cryst. Growth* **237** 2019
[15] Carlsson E A, Zunger A and Wood M D 1985 *Phys. Rev.* B **32** 1386
[16] Yu H L, Yao L K and Liu L Z 2004 *Physica* B **353** 278
[17] Blöchl E P 1994 *Phys. Rev.* B **50** 17953
[18] Kresse G and Hafner J 1993 *Phys. Rev.* B **47** RC558
[19] Kresse G and Hafner J 1993 *Phys. Rev.* B **48** 13115
[20] Kresse G and Hafner J 1994 *Phys. Rev.* B **49** 14251
[21] Kresse G and Furthmuller J 1996 *Comput. Mater. Sci.* **6** 15
[22] Kresse G and Furthmuller J 1996 *Phys. Rev.* B **54** 11169
[23] Perdew P J, Burke K and Ernzerhof M 1996 *Phys. Rev. Lett.* **77** 3865
[24] Monkhorst J H and Pack D J 1976 *Phys. Rev.* B **13** 5188
[25] Feynman P R 1939 *Phys. Rev.* **56** 340
[26] Van de Walle G C and Neugebauer J 2004 *J. Appl. Phys.* **95** 3851
[27] Matsunaga K, Tanaka T, Yamamoto T and Ikuhara Y 2003 *Phys. Rev.* B **68** 85110
[28] Parlinski K, Li Q Z and Kawazoe Y 1997 *Phys. Rev. Lett.* **78** 4063
[29] Chase W M Jr 1998 *NIST-JANAF Themochemical Tables* (*J. Phys. Chem. Ref. Data, Monograph* vol 9) 4th edn, p 1621